Measurements of the parameters of the $\phi(1020)$ resonance through studies of the processes $e^+e^- \to K^+K^-$, K_SK_L, and $\pi^+\pi^-\pi^0$

M. N. Achasov,* K. I. Beloborodov, A. V. Berdyugin, A. G. Bogdanchikov, A. V. Bozhenok, A. D. Bukin, D. A. Bukin, S. V. Burdin, T. V. Dimova, V. P. Druzhinin, M. S. Dubrovin, I. A. Gaponenko, V. B. Golubev, V. N. Ivanchenko, P. M. Ivanov, A. A. Korol, M. S. Korostelev, S. V. Koshuba, E. V. Pakhtusova, A. A. Polunin, E. E. Pyata, A. A. Salnikov, S. I. Serednyakov, V. V. Shary, Yu. M. Shatunov, V. A. Sidorov, Z. K. Silagadze, A. N. Skrinsky, Yu. V. Usov, A. V. Vasiljev, and Yu. S. Velikzhanin

Budker Institute of Nuclear Physics, Siberian Branch of the Russian Academy of Sciences and Novosibirsk State University, 11 Laurentyev, Novosibirsk, 630090, Russia

(Received 15 September 2000; published 6 March 2001)

The cross sections of the processes $e^+e^- \to K^+K^-$, $e^+e^- \to K_SK_L$, and $e^+e^- \to \pi^+\pi^-\pi^0$ were measured in the SND experiment at the VEPP-2M collider in the energy region near the $\phi(1020)$ meson. These measurements were based on about 10^6 K^+K^-, 0.5×10^6 K_SK_L, and 0.4×10^6 $\pi^+\pi^-\pi^0$ selected events. The measured cross sections have been analyzed in the framework of the vector meson dominance model and the main parameters of the ϕ resonance were obtained, such as its mass, width, the production cross section, and branching ratios of the main decay modes. The measured value of the ϕ meson total width, $\Gamma_\phi = 4.21 \pm 0.04$, is lower than the present world average of 4.458 ± 0.032 MeV. Contributions in addition to the conventional vector meson dominance model were found in the $e^+e^- \to \pi^+\pi^-\pi^0$ reaction cross section.

DOI: 10.1103/PhysRevD.63.072002 PACS number(s): 13.65.+i, 12.40.Vv, 13.25.Jx, 14.40.Cs

I. INTRODUCTION

Cross sections of the reactions $e^+e^- \to K\bar{K}$ and $e^+e^- \to \pi^+\pi^-\pi^0$ are determined by strong and electromagnetic interactions of the light quarks (s,u,d) and cannot be evaluated at present from first principles. But a rather good description of these cross sections is provided by the vector meson dominance model (VDM) with phenomenologically adjusted coupling constants ($g_{V\gamma}$, $g_{V\rho\pi}$, $g_{VP\gamma}$, g_{VPP}). In the VDM, the cross sections are determined by the amplitudes of vector meson V transitions ($V=\phi$, ω, ρ) into the final state: $V \to \rho\pi \to 3\pi$, $V \to K\bar{K}$. In the energy range from 980 to 1070 MeV, the main contributions to the $e^+e^- \to K\bar{K}$ and $e^+e^- \to \pi^+\pi^-\pi^0$ cross sections come from the ϕ meson. Therefore the measurement of these cross sections allows us to determine the ϕ resonance main parameters and study its interference with other vector mesons. Such studies provide important information about light meson physics.

Earlier, these processes were studied in several experiments: $e^+e^- \to 3\pi$ [1–6], and $e^+e^- \to K_SK_L$ [4,5,7,8], $e^+e^- \to K^+K^-$ [5,9,10]. The SND (Spherical Neutral Detector) experiment continues these efforts at the VEPP-2M collider [11]. Here we present the results of this investigation.

II. EXPERIMENT

SND has been operating at the VEPP-2M collider in the energy range from 360 to 1400 MeV since 1995 (the SND detailed description can be found in Ref. [12]). The detector contains several subsystems. The tracking system includes two cylindrical drift chambers. The three-layer spherical electromagnetic calorimeter is based on NaI(Tl) crystals. The muon or veto system consists of plastic scintillation counters and two layers of streamer tubes. The calorimeter energy and angular resolution depend on the photon energy as $\sigma_E/E(\%) = 4.2\%/\sqrt[4]{E(\mathrm{GeV})}$ and $\sigma_{\phi,\theta} = 0.82°/\sqrt{E(\mathrm{GeV})} \oplus 0.63°$. The tracking system angular resolution is about 0.5° and 2° for azimuthal and polar angles, respectively. The energy loss resolution dE/dx in the drift chamber is about 30%—good enough to provide charged kaon identification in the region of ϕ-meson production.

This work is based on the data sample collected in the SND experiments during 1998. The data were collected at 32 energy points in the energy range from 984 to 1060 MeV (Table I). The total integrated luminosity accumulated in these experiments is 8.5 pb^{-1}. The beam energy was calculated from the magnetic field value in the bending magnets and revolution frequency of the collider. In the vicinity of the ϕ-meson peak we also used the beam energy calibrated by the Cryogenic Magnetic Detector (CMD-2), which operated at VEPP-2M at the same time. This calibration [8,13] is based on the measurements of the charged kaon momenta in the drift chamber of CMD-2. The energy calibration accuracy in each point is about 0.1 MeV, the common shift of the energy scale is estimated to be 0.04 MeV, and the energy spread of the beams is about 0.37 MeV.

For the luminosity measurements, $e^+e^- \to e^+e^-$ and $e^+e^- \to \gamma\gamma$ processes were used. The corresponding luminosity values were, respectively, used for normalizing the events containing charged particles and those with neutral particles only. They are different by about 10% (Table I) due to the dead time of the trigger, which selected events containing neutral particles only. The systematic error of the integrated luminosity determination is estimated to be 2%. Since luminosity measurements by $e^+e^- \to e^+e^-$ and $e^+e^- \to \gamma\gamma$ reveal a systematic spread of about 1.3%, this was added to the statistical error of the luminosity determi-

*Email address: achasov@inp.nsk.su

TABLE I. Experimental main parameters: $\sqrt{s}$, the energy in the center-of-mass system; σ, beam energy spread; IL_{cha}, IL_{neu}, integrated luminosities used for normalizing the events containing charged particles and with neutral particles only.

Scan PHI9801				Scan PHI9802			
$\sqrt{s}$ (MeV)	σ (MeV)	IL_{cha} (nb^{-1})	IL_{neu} (nb^{-1})	$\sqrt{s}$ (MeV)	σ (MeV)	IL_{cha} (nb^{-1})	IL_{neu} (nb^{-1})
984.21±0.10	0.36	173.7±2.3	159.7±2.4	984.02±0.10	0.36	200.9±2.7	186.7±2.7
1003.91±0.10	0.36	209.9±2.8	193.6±2.8	1003.71±0.10	0.36	181.1±2.4	171.4±2.6
1010.17±0.13	0.37	156.0±2.1	140.8±2.2	1010.34±0.13	0.37	158.1±2.1	147.6±2.2
1015.75±0.07	0.37	168.2±2.2	160.1±2.4	1015.43±0.07	0.39	200.9±2.7	183.7±2.7
1016.68±0.07	0.37	304.7±4.0	286.8±4.1	1016.78±0.07	0.38	333.0±4.4	299.1±4.2
1017.59±0.07	0.37	483.3±6.3	444.2±6.1	1017.72±0.07	0.37	528.4±6.9	478.7±6.6
1018.78±0.07	0.38	527.0±6.9	482.8±6.6	1018.62±0.07	0.38	536.5±7.0	484.1±6.6
1019.79±0.07	0.37	560.2±7.3	511.4±7.0	1019.51±0.07	0.37	523.6±6.9	472.7±6.5
1020.65±0.08	0.37	323.7±4.3	296.3±4.2	1020.43±0.08	0.37	355.6±4.7	330.7±4.6
1021.68±0.08	0.37	163.2±2.2	150.4±2.3	1021.41±0.08	0.37	184.3±2.4	172.1±2.6
1023.27±0.09	0.37	202.6±2.7	186.2±2.8	1022.32±0.09	0.39	178.1±2.4	166.3±2.5
1028.23±0.14	0.37	167.9±2.2	150.1±2.3	1027.52±0.14	0.38	218.4±2.9	211.5±3.1
1033.84±0.10	0.37	167.8±2.2	147.7±2.3	1033.58±0.10	0.36	182.2±2.4	172.3±2.6
1039.59±0.10	0.39	162.7±2.1	151.5±2.3	1039.64±0.10	0.37	185.1±2.5	169.2±2.5
1049.81±0.10	0.38	196.9±2.6	178.9±2.7	1049.60±0.10	0.38	187.2±2.5	176.3±2.6
1059.66±0.10	0.38	169.8±2.3	158.6±2.4	1059.52±0.10	0.50	216.3±2.9	205.6±3.0

nation in each energy point. The statistical accuracy was better than 1%.

The experimental conditions were rather stable during data taking: the SND systems counting rate, average currents, and luminosity of the collider were stable at the level of about 20% and no correlation between different energy points was observed.

III. DATA ANALYSIS

The procedure of the experimental data selection consists of several stages. During the experimental runs, the first-level trigger was used [12]. The first-level trigger selects events of different types: events with photons only and events with charged particles. The thresholds applied on the energy deposition in the calorimeter were about 200 MeV for events containing charged particles and 300 MeV for events with neutral particles only.

During the processing of experimental data, the event reconstruction is performed in the following sequence. The first step is a search for separated clusters in the calorimeter. Track reconstruction in the drift chambers is then performed. Tracks are linked to the calorimeter clusters. Clusters with energy depositions of more than 20 MeV, and not linked to tracks in the drift chambers, are considered as photons. For charged tracks no requirements on the energy depositions in the calorimeter are imposed.

For further analysis, events with $|z|<10$ cm and $r<1$ cm for each charged particle were selected. Here z is the coordinate of the charged particle production point along the beam axis (the longitudinal size of the interaction region is $\sigma_z \sim 2.5$ cm); r is the distance between a charged particle track and the beam axis in the $r-\phi$ plane. For each process individual selection criteria were then applied.

The detection efficiency was obtained from Monte Carlo (MC) simulation. Simulated events were reconstructed and the actual selection criteria were applied. To take into account the apparatus resolution of the first-level trigger thresholds, for simulated and experimental events the trigger conditions were applied with the threshold values 10% higher than during the experimental runs.

As a result of uncertainties in the simulation of the distributions over some selection parameters, the detection efficiency was multiplied by correction coefficients, which were obtained in the following way. The experimental events were selected without any conditions on the parameter under study, using the cut parameters uncorrelated with the studied one. The same selection was applied for simulated events. Then the cut was applied to the parameter and the correction coefficient was calculated:

$$\delta = \frac{n/N}{m/M}, \tag{1}$$

where N and M are the number of events in experiment and simulation selected without any cuts on the parameter under study; n and m are the number of events in experiment and simulation, when the cut on the parameter was applied. As a rule, the error in the coefficient δ determination is connected with the uncertainty of background subtraction. This systematic error was estimated by varying other selection criteria.

The overlap of the beam background with the events containing charged particles can result in track reconstruction failure and a decrease of detection efficiency. To take into account this effect, background events (experimental events collected when detector was triggered with an external gen-

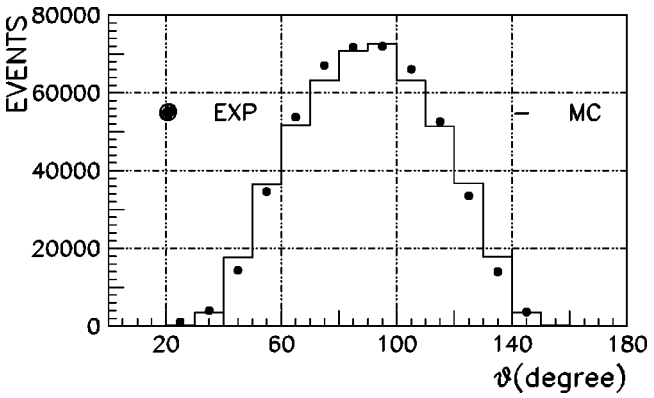

FIG. 1. The θ distribution of charged particles from the $e^+e^- \to K^+K^-$ reaction.

erator) were overlapped with the simulated events. It was found that the detection efficiency decreased by about 3% and therefore the correction coefficient $\delta_{over}=0.97\pm0.03$ was used for the processes containing charged particles. In the analysis described further simulated events are not overlapped with beam background events.

A. Selection of $e^+e^- \to K^+K^-$ events

In the studied energy region the $e^+e^- \to K^+K^-$ events have the following features:

(i) The charged kaons are rather slow ($\beta\gamma \sim 0.2$–0.4) and therefore have large dE/dx losses in the drift chamber.

(ii) Events often contain several photons due to the kaon decays ($K^\pm \to \pi^\pm\pi^0$, $\pi^\pm\pi^0\pi^0$, $\pi^0\mu^\pm\nu_\mu$, $\pi^0 e^\pm \nu_e$) in the tracking system.

(iii) Tracks attributed to the kaon decays in the tracking system (secondary particles) are also present.

To select the $e^+e^- \to K^+K^-$ events, detection of two charged particles was required, with polar angles in the range $20° < \theta < 160°$, with acollinearity angle in the azimuthal plane $\Delta\phi < 10°$ and the energy losses in the drift chamber $dE/dx > 3(dE/dx)_{min}$, where $(dE/dx)_{min}$ is an average (dE/dx) loss of a minimum ionizing particle. The events must also contain two or more photons and at least one secondary particle from kaon decay in the tracking system. The distribution of the angle θ for charged particles in the selected events has the typical shape for the $e^+e^- \to K^+K^-$ reaction (Fig. 1).

After these cuts, the background processes $e^+e^- \to \pi^+\pi^-$, $\mu^+\mu^-$ and also beam and cosmic backgrounds still contribute. The data accumulated under the $K\bar{K}$ production threshold, at the energy point $\sqrt{s}=984$ MeV, were used to estimate the number of background events. After selection criteria were applied, only $N_{bkg}(984)=5$ events were found at this point. The number of background events in each energy point was calculated as

$$N_{bkg}(s) = N_{bkg}(984)\frac{IL(s)}{IL(984)}, \tag{2}$$

where $IL(s)$ is the integrated luminosity, and this number was subtracted from the number of selected events.

The detection efficiency was multiplied by correction coefficients: $\delta_{dE/dx}$, δ_{over}, δ_{NP}, δ_{etot}. Here $\delta_{dE/dx}=0.93\pm0.02$ is a correction due to the inaccuracy in the simulation of the dE/dx distributions. This coefficient does not depend on the energy in the explored region. The coefficient δ_{NP} is a correction to the efficiency of detection of secondary particles and at least two photons. Its value varies in this energy range by $\sim$ 10% and in the vicinity of the ϕ-resonance peak is $\delta_{NP}=0.99\pm0.015$. The correction $\delta_{etot}=0.91\pm0.05$ is due to the inaccuracy in the simulation of the average energy deposition of $e^+e^- \to K^+K^-$ events. The total systematic error of the detection efficiency determination is 6.8%. The number of selected $e^+e^- \to K^+K^-$ events (after background subtraction) and the detection efficiency are shown in Table II. The detection efficiency rises with energy because the probability of kaon absorption in the detector passive mate-

TABLE II. Event numbers N and detection efficiencies ϵ for the $e^+e^- \to K^+K^-$ process versus energy.

Scan PHI9801			Scan PHI9802		
$\sqrt{s}$ (MeV)	$N_{K^+K^-}$	$\epsilon_{K^+K^-}$	$\sqrt{s}$ (MeV)	$N_{K^+K^-}$	$\epsilon_{K^+K^-}$
1010.17	306±23	0.055±0.012	1010.34	272±22	0.0599±0.012
1015.75	8370±108	0.1669±0.0045	1015.43	8524±110	0.1638±0.0045
1016.68	27723±195	0.1749±0.0046	1016.78	31181±207	0.1758±0.0046
1017.59	69921±321	0.1814±0.0047	1017.72	72263±325	0.1821±0.0047
1018.78	124598±431	0.1878±0.0049	1018.62	121718±421	0.1869±0.0048
1019.79	149331±472	0.1922±0.0049	1019.51	139295±452	0.1909±0.0049
1020.65	73994±321	0.1958±0.005	1020.43	88199±342	0.1948±0.005
1021.68	26342±187	0.2001±0.0052	1021.41	33916±211	0.1992±0.0051
1023.27	20637±167	0.2037±0.0053	1022.32	22111±169	0.2021±0.0052
1028.23	7009±97	0.2115±0.0059	1027.52	9865±112	0.2106±0.0059
1033.84	3747±72	0.2163±0.0064	1033.58	4437±75	0.2164±0.0064
1039.59	2349±52	0.1975±0.0063	1039.64	2745±58	0.1972±0.0063
1049.81	1270±40	0.1330±0.005	1049.6	1298±40	0.1334±0.005
1059.66	672±27	0.1228±0.0053	1059.52	961±33	0.1233±0.0053

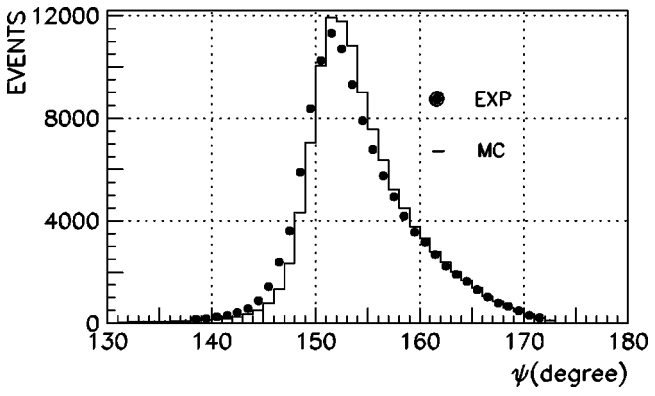

FIG. 2. Angle ψ between pion pairs from the $K_S \to \pi^+\pi^-$ decay.

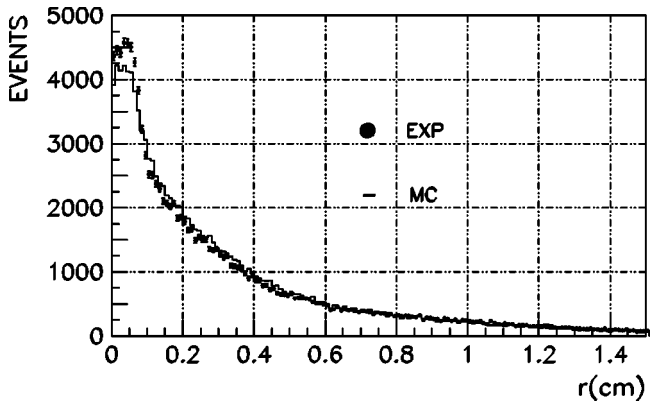

FIG. 3. The r distribution of pions from the $K_S \to \pi^+\pi^-$ decay.

rial decreases with energy. Above 1035 MeV the efficiency goes down since the probability of kaon decay in the detector decreases.

B. Selection of $e^+e^- \to K_S K_L$ events

The K_S and K_L mesons decay lengths in the studied energy region are $c\tau\beta\gamma \sim 0.3$–1 cm and 2–5.6 m, respectively. The K_S meson decays inside the collider vacuum chamber or tracking system, and the K_L reaches the calorimeter, where it can either produce signals (''photons'') due to nuclear interactions or decay in flight, or it can pass through the detector without interacting. The analysis of the $e^+e^- \to K_S K_L$ reaction is based on the detection of $K_S \to \pi^+\pi^-$ or $K_S \to \pi^0\pi^0$ decays.

In the first case (charged mode) the events which contained two charged particles and at least one ''photon'' were used. The polar angles of the charged particles and their acollinearity angle were bounded by the criteria $36° < \theta < 144°$, $|\Delta\theta| < 30°$, and $10° < |\Delta\phi| < 50°$. The cut $10° < |\Delta\phi|$ rejects the background from $e^+e^- \to K^+K^-$ events. To suppress the same background, the following cuts were also applied: $(dE/dx) < 5(dE/dx)_{min}$ for each charged particle and $(dE/dx) < 3(dE/dx)_{min}$ at least for one.

The K_S meson decay length is about 0.5 cm, so to suppress the background from $e^+e^- \to 3\pi$, $\eta\gamma(\eta \to \pi^+\pi^-\pi^0, \pi^+\pi^-\gamma)$, $\omega\pi^0$, $e^+e^-\gamma\gamma$ events, the cut 0.2 cm $< r < 1$ was used. The beam and cosmic backgrounds were suppressed by the criteria $E_p > 0$ and $E_{p3} < 50$ MeV, where E_p and E_{p3} are the total energy deposition and the energy deposition in the third calorimeter layer of any charged particle. Pions in the process under study have energies of about ~ 200–300 MeV and actually give a very low energy deposition in the third layer. The distribution of the angle ψ between charged particles in the selected events is shown in Fig. 2. It has a characteristic peak at the minimum angle between pions, close to 150°.

To estimate the number of background events, the data accumulated at the energy point $\sqrt{s} = 984$ MeV, i.e., under the reaction threshold, were used. After the cuts, $N_{bkg}(984) = 30$ events were left. Their production points are uniformly distributed along the beam direction, so these events can be attributed to the beam and cosmic backgrounds. The number of background events in other energy points was calculated according to the formula (2) and then subtracted from the number of selected events.

The detection efficiency was multiplied by correction coefficients $\delta_{dE/dx}$, δ_{over}, and δ_r. Here $\delta_{dE/dx} = 0.95 \pm 0.01$ is a correction due to an inaccuracy in the simulation of the dE/dx distribution. The coefficient δ_r is a correction due to an inaccuracy in the simulation of the r distribution (Fig. 3). Its value varies in this energy region by $\sim$ 10% and in the vicinity of the ϕ-resonance peak is $\delta_r = 0.91 \pm 0.015$. The total systematic error of the detection efficiency determination is 3.7%. The numbers of selected $e^+e^- \to K_S K_L$ events (after background subtraction) and the detection efficiencies are shown in Table III. The detection efficiency depends on the energy due to the dependence of $\Delta\phi$ and $\Delta\theta$ distributions on the K_S energy and the dependence of K_L nuclear interactions and decay length on its energy.

For analysis of the $e^+e^- \to K_S K_L$ decay in the neutral mode ($K_S \to \pi^0\pi^0$), we used events where at least four photons were detected and no charged particles were present. To reject beam and cosmic backgrounds, constraints were imposed on the total energy deposition ($E_{tot} > 0.35\sqrt{s}$) and total momentum of events ($P_{tot} < 0.6\sqrt{s}$). To suppress cosmic background even further, the events where most of the hit crystals could be fitted by a single track were rejected.

For events satisfying selection criteria described above, the kinematic fit was performed under the following assumptions: the event contains two photon pairs originating from the $\pi^0 \to \gamma\gamma$ decay and invariant mass of these four photons is equal to the K_S-meson mass. The value of the likelihood function $\chi^2_{K_S}$ is calculated. In events with more than four photons, extra photons are considered as spurious ones and rejected. To do this, all possible subsets of four photons were tested and one, corresponding to the maximum likelihood, was selected. Figures 4 and 5 represent invariant masses of photon pairs and of all four photons found in the reconstruction. To suppress the beam background, polar angles of the photons, reconstructed as γ quanta from the $K_S \to 2\pi^0 \to 4\gamma$ decay, were limited to $40° < \theta < 140°$. The background from the multiphoton events (pure QED events, $e^+e^- \to \pi^0\pi^0\gamma$ and $\eta\gamma$) was rejected by the following cuts: $\chi^2_{K_S}$

TABLE III. Event numbers N and detection efficiencies ϵ for the $e^+e^-\to K_SK_L$ process with $K_S\to\pi^+\pi^-$ decay.

Scan PHI9801			Scan PHI9802		
$\sqrt{s}$ (MeV)	$N_{K_SK_L}$	$\epsilon_{K_SK_L}$	$\sqrt{s}$ (MeV)	$N_{K_SK_L}$	$\epsilon_{K_SK_L}$
1003.91	56±9	0.0475±0.019	1003.71	46±9	0.0469±0.019
1010.17	277±18	0.532±0.0069	1010.34	249±17	0.0534±0.0069
1015.75	2372±50	0.0614±0.0028	1015.43	2594±53	0.0614±0.0028
1016.68	7092±88	0.0612±0.0016	1016.78	8314±95	0.0612±0.0016
1017.59	18335±141	0.0634±0.0011	1017.72	19545±145	0.0632±0.0011
1018.78	30820±182	0.0631±0.0011	1018.62	31703±185	0.0631±0.0011
1019.79	36358±198	0.0636±0.0012	1019.51	35272±195	0.0636±0.0012
1020.65	17276±137	0.0632±0.0011	1020.43	21071±150	0.0633±0.0011
1021.68	5975±80	0.0642±0.0019	1021.41	7726±90	0.0643±0.0019
1023.27	4453±69	0.0633±0.0022	1022.32	4895±72	0.0637±0.0022
1028.23	1361±39	0.0627±0.0035	1027.52	2079±47	0.0630±0.0035
1033.84	679±27	0.0607±0.0043	1033.58	901±31	0.0608±0.0043
1039.59	471±23	0.0620±0.0057	1039.64	517±24	0.062±0.0056
1049.81	311±19	0.0633±0.0074	1049.60	330±20	0.062±0.0073
1059.66	234±17	0.0395±0.0069	1059.52	245±17	0.0395±0.0069

<20 and $\Delta p<100$ MeV. Here $\Delta p=p_{K_S}-\sqrt{s/4-m_{K_S}^2}$ and p_{K_S} is the measured kaon momentum. The $\chi^2_{K_S}$ and p_{K_S} distributions are shown in Figs. 6, 7, and 8.

After these cuts were applied, only three events were found at the energy point $\sqrt{s}=984$ MeV. The number of background events for each energy point was calculated according to Eq. (2) and then subtracted from the number of selected events. The number of background events from the $e^+e^-\to\eta\gamma$ decay was estimated using simulation, and even in the vicinity of the ϕ-resonance peak, their number is less than 0.2% of the selected $e^+e^-\to K_SK_L$ events.

The detection efficiency was multiplied by correction coefficients δ_θ and $\delta_{\chi^2_{K_S}}$. The $\delta_{\chi^2_{K_S}}=0.97\pm0.01$ is a correction due to an inaccuracy in the simulation of the $\chi^2_{K_S}$ distribution. The experimental $e^+e^-\to K_SK_L$ events can contain false photons, caused by the beam background overlaps. The energy of these photons is similar to the energy of the γ quanta from the K_S decay, and they are localized at the polar angles close to the beam direction. During reconstruction, some false photons can be mistaken as originating from the K_S decay. In other words, the reconstruction program can reject with some probability a valid photon from the K_S decay and substitute it by the false one. An event reconstructed in such a way will not pass our cut on the photon polar angles (described above) because the beam related false photons have small polar angles. Therefore the beam background overlaps lead to the decrease of the detection efficiency—an effect not taken into account in the MC simulation. Hence the necessity of the correction coefficient $\delta_\theta=0.90\pm0.03$ arises. The detection efficiency does not depend on the energy and equals 0.068 after all corrections were implemented. The total systematic error of the detection efficiency determination is 3.5%. The selected event

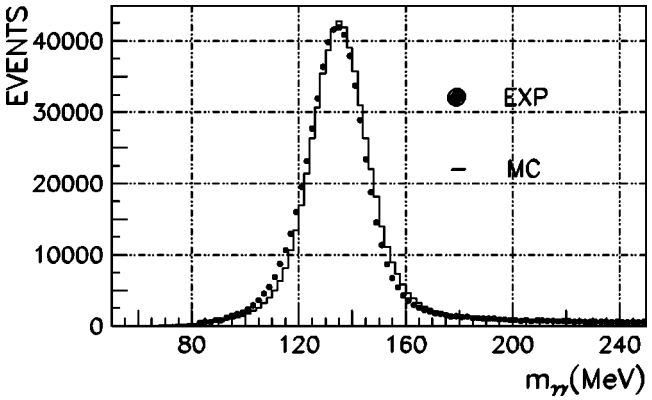

FIG. 4. The invariant mass of photon pairs from the $K_S\to\pi^0\pi^0$ decay.

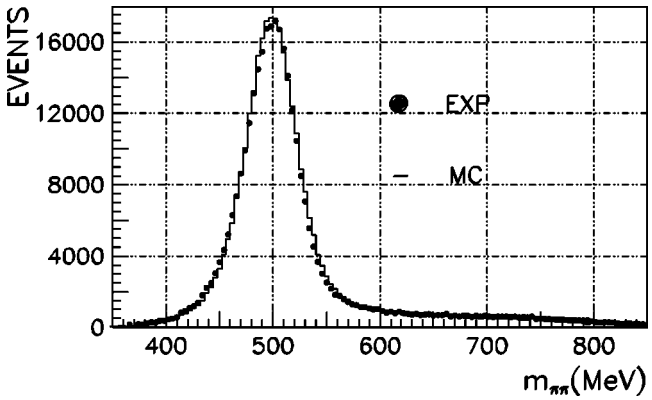

FIG. 5. The invariant mass of pions from the $K_S\to\pi^0\pi^0$ decay.

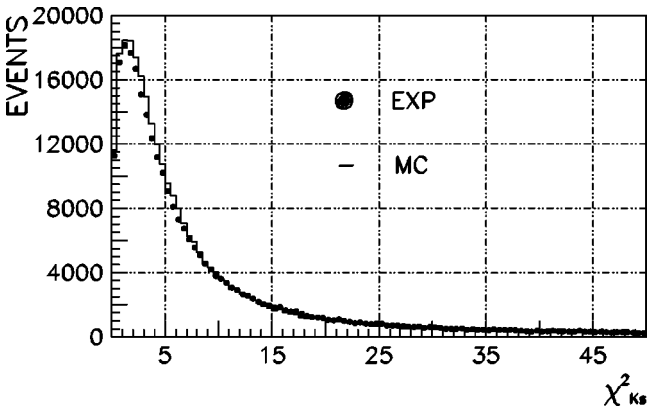

FIG. 6. The $\chi^2_{K_S}$ distribution for the $K_S\to\pi^0\pi^0$ events.

numbers (after background subtraction) are shown in Table IV.

C. Selection of $e^+e^-\to\pi^+\pi^-\pi^0$ events

For analysis of the $e^+e^-\to\pi^+\pi^-\pi^0$ process, events containing two charged particles and two or more photons were used. Extra photons can appear because of the beam background overlap, splitting of the electromagnetic showers, and nuclear interactions of the charged pions in the calorimeter. Under these selection conditions, the background sources are $e^+e^-\to K^+K^-$, $K_SK_L(K_S\to\pi^+\pi^-)$, $\eta\gamma(\eta\to\pi^+\pi^-\pi^0$, $\pi^+\pi^-\gamma)$, $\omega\pi^0$, $e^+e^-\gamma\gamma$ processes and the beam background.

The polar angles of the charged particles were bounded by the criterion $20°<\theta<160°$. To suppress the beam background, the following cuts on the spatial angle between two charged particles and energy deposition of the neutral particles were applied: $\psi>40°$, $E_{neu}>0.1\sqrt{s}$.

To suppress the background from the $e^+e^-\to K^+K^-$ process, the following cuts were imposed: $(dE/dx)<5(dE/dx)_{min}$ for each charged particle, $(dE/dx)<3(dE/dx)_{min}$ at least for one, and $\Delta\phi<10°$. To reject the $e^+e^-\to e^+e^-\gamma\gamma$ events the energy deposition of the charged particles was bounded by the criterion $E_{cha}<0.5\sqrt{s}$.

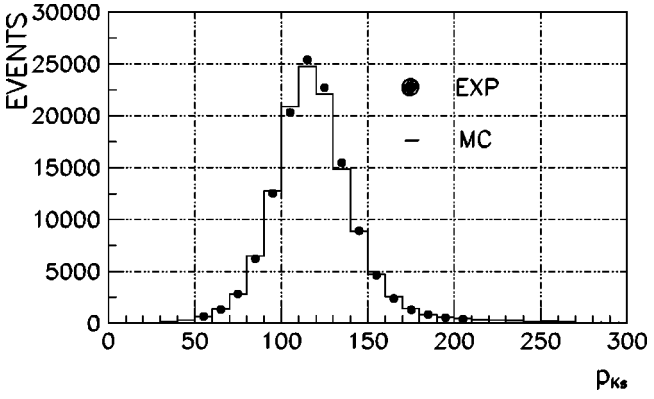

FIG. 7. The kaon momentum distribution from the $K_S\to\pi^0\pi^0$ decay at the energy $\sqrt{s}=1020$ MeV.

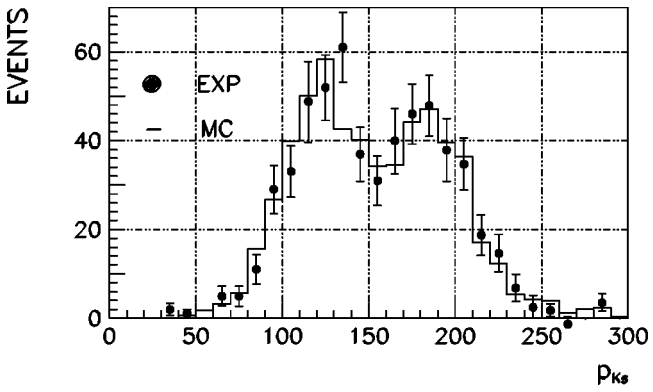

FIG. 8. The kaon momentum distribution from the $K_S\to\pi^0\pi^0$ decay at the energy $\sqrt{s}=1060$ MeV. The left peak corresponds to the case when the photon was emitted by the initial particles.

For events left after these cuts, a kinematic fit was performed under the following constraints: the charged particles are considered to be pions, the system has zero momentum, the total energy is $\sqrt{s}$, and the photons originate from the $\pi^0\to\gamma\gamma$ decays. The value of the likelihood function $\chi^2_{3\pi}$ is calculated. In events with more than two photons, extra photons are considered as spurious ones and rejected. To do this, all possible subsets of two photons were tested and the one corresponding to the maximum likelihood was selected. Two-photon invariant mass and $\chi^2_{3\pi}$ distributions are shown in Figs. 9 and 10. After the kinematic fit, the following additional cuts were applied: $36°<\theta_\gamma<144°$, $NNP=2$, and $\chi^2_{3\pi}<20$ for energy points with $\sqrt{s}<1028$ MeV and $\chi^2_{3\pi}<5$ for energy points above 1028 MeV. Here θ_γ is polar angle of any photon selected by the reconstruction program as originated from the π^0 decay. NNP is the number of detected photons. A harder cut on $\chi^2_{3\pi}$ at the five last energy points is necessary to suppress $e^+e^-\to3\pi\gamma_{rad}$ events,

TABLE IV. Event numbers N for the $e^+e^-\to K_SK_L$ process with $K_S\to\pi^0\pi^0$ decay.

Scan PHI9801		Scan PHI9802	
$\sqrt{s}$ (MeV)	$N_{K_SK_L}$	$\sqrt{s}$ (MeV)	$N_{K_SK_L}$
1003.91	74±9	1003.71	57±8
1010.17	241±16	1010.34	250±16
1015.75	2340±50	1015.43	2431±51
1016.68	7267±87	1016.78	7865±90
1017.59	17558±135	1017.72	20422±146
1018.78	29870±176	1018.62	29376±175
1019.79	35002±190	1019.51	32910±185
1020.65	16908±132	1020.43	20454±145
1021.68	5968±79	1021.41	7680±89
1023.27	4463±68	1022.32	4945±72
1028.23	1376±38	1027.52	2187±48
1033.84	767±28	1033.58	936±31
1039.59	521±24	1039.64	559±24
1049.81	372±20	1049.60	390±20
1059.66	234±16	1059.52	333±19

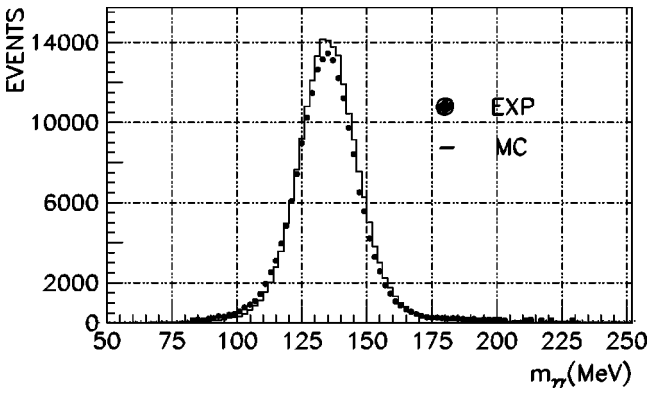

FIG. 9. Two-photon invariant mass distribution in the $\phi \to \pi^+\pi^-\pi^0$ events.

where γ_{rad} is a photon emitted by initial particles.

As experimental data were accumulated in a rather narrow energy region, the detection efficiency for the events without γ-quantum radiation by initial particles does not depend on energy in the entire region. The detection efficiency dependence on the radiated photon energy, obtained from simulation, is shown in Fig. 11.

The detection efficiency was multiplied by correction coefficients δ_{over}, $\delta_{dE/dx}=0.95\pm0.01$, $\delta_{\chi^2_{3\pi}}=0.93\pm0.03$, and $\delta_{NNP}=0.87\pm0.005$. The last correction factor is due to inaccuracies in the simulation of extra photons. The detection efficiency (without γ-quantum radiation) equals 0.183 (under condition $\chi^2_{3\pi}<20$) and 0.086 (under the condition $\chi^2_{3\pi}<5$) after all corrections were implemented. The total systematic error of the detection efficiency determination is 4.5%. The selected event numbers are shown in Table IV.

The number of background events ($e^+e^-\to\omega\pi^0$, $\eta\gamma$, $e^+e^-\gamma\gamma$ and $K\bar{K}$) was estimated using simulation in the following way:

$$N_{bkg}(s)=\sum_i \sigma_{Ri}(s)\epsilon_i(s)\delta_i IL(s), \qquad (3)$$

where i is a background process number, $\sigma_{Ri}(s)$ is the cross section of the process taking into account the radiative corrections, $IL(s)$ is the integrated luminosity, $\epsilon_i(s)$ is the detection efficiency, and δ_i is a correction to the efficiency. For $e^+e^-\to K\bar{K}$ reactions the $\sigma_{Ri}(s)$ were taken according to the SND measurements presented in this article and for the process $e^+e^-\to\omega\pi^0$ other SND measurements [14] were used. The $e^+e^-\to K_SK_L$ is the main background in the vicinity of the ϕ-resonance peak ($\sqrt{s}=1015.75$–1028.23 MeV) and its contribution is $\sim$90% of all background. Outside this region the background is strongly determined by the $e^+e^-\to\omega\pi^0$ and $e^+e^-\gamma\gamma$ events. The background from the $e^+e^-\to K^+K^-$ events is negligible, and even at the ϕ-meson peak it is only $\sim$0.5% of all background events. The accuracy of background event number determination is less than 15% at

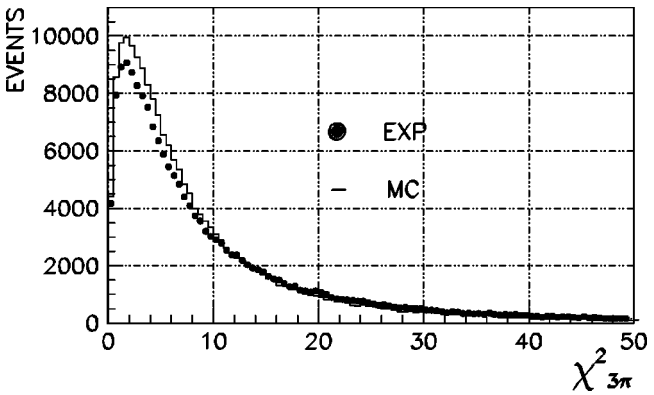

FIG. 10. The $\chi^2_{3\pi}$ distribution in $e^+e^-\to\pi^+\pi^-\pi^0$ events.

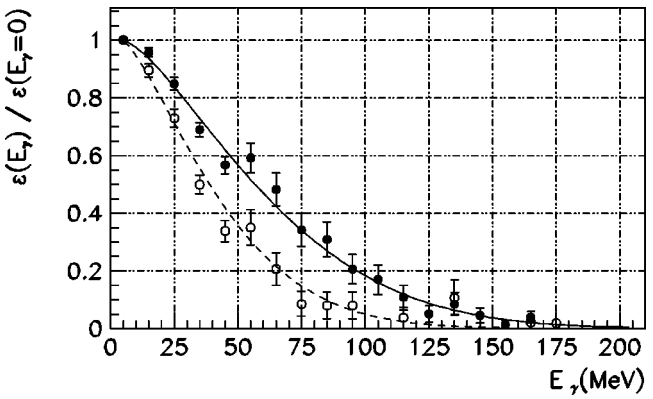

FIG. 11. The detection efficiency $\epsilon(E_\gamma)$ dependence on the radiated photon energy E_γ for $e^+e^-\to3\pi+\gamma$ events under the conditions $\chi^2_{3\pi}<20$ (dots) and $\chi^2_{3\pi}<5$ (circles), obtained by simulation.

TABLE V. Event numbers $N_{3\pi}$ and N_{bkg} of the $e^+e^-\to\pi^+\pi^-\pi^0$ (after background subtraction) and background processes respectively. The accuracy of background event numbers determination is less than 15% at all energy points.

Scan PHI9801			Scan PHI9802		
$\sqrt{s}$ (MeV)	$N_{3\pi}$	N_{bkg}	$\sqrt{s}$ (MeV)	$N_{3\pi}$	N_{bkg}
984.21	498±23	5	984.02	552±25	5
1003.91	1145±36	8	1003.71	1026±34	7
1010.17	1548±42	11	1010.34	1592±43	12
1015.75	5610±79	52	1015.43	6094±83	55
1016.68	14833±129	154	1016.78	15956±133	177
1017.59	31862±190	394	1017.72	36261±202	458
1018.78	45502±228	657	1018.62	46722±230	643
1019.79	46590±229	770	1019.51	47414±232	735
1020.65	20172±151	381	1020.43	25387±169	448
1021.68	6339±86	144	1021.41	8588±99	180
1023.27	4160±69	104	1022.32	4969±76	121
1028.23	444±22	4	1027.52	715±27	5
1033.84	203±16	3	1033.58	254±16	4
1039.59	118±12	2	1039.64	133±12	2
1049.81	91±12	2	1049.60	87±9	2
1059.66	54±8	4	1059.52	66±8	5

all energy points. The obtained number $N_{bkg}(s)$ was subtracted from the selected events. The numbers of the $e^+e^- \to 3\pi$ and background events are shown in Table V.

IV. THEORETICAL CROSS SECTIONS

In the VDM framework the cross sections of the $e^+e^- \to K^+K^-$, K_SK_L and $\pi^+\pi^-\pi^0$ process are written as follows [15]:

$$\sigma_{K^+K^-}(s)=\frac{8\pi\alpha}{3s^{5/2}}q^3_{K^+K^-}(s)\left|\frac{g_{\phi\gamma}g_{\phi K^+K^-}}{D_\phi(s)}e^{i\phi_{K\bar{K}}}-\frac{g_{\omega\gamma}g_{\omega K^+K^-}}{D_\omega(s)}-\frac{g_{\rho\gamma}g_{\rho K^+K^-}}{D_\rho(s)}+A_{K^+K^-}\right|^2, \tag{4}$$

$$\sigma_{K_SK_L}(s)=\frac{8\pi\alpha}{3s^{5/2}}q^3_{K_SK_L}(s)\left|\frac{g_{\phi\gamma}g_{\phi K_SK_L}}{D_\phi(s)}e^{i\phi_{K\bar{K}}}-\frac{g_{\omega\gamma}g_{\omega K_SK_L}}{D_\omega(s)}+\frac{g_{\rho\gamma}g_{\rho K_SK_L}}{D_\rho(s)}+A_{K_SK_L}\right|^2, \tag{5}$$

$$\sigma_{3\pi}(s)=\frac{4\pi\alpha}{s^{3/2}}W(s)\left|\frac{g_{\phi\gamma}g_{\phi\rho\pi}}{D_\phi(s)}e^{i\chi_{\phi-\omega}}+\frac{g_{\omega\gamma}g_{\omega\rho\pi}}{D_\omega(s)}+A_{3\pi}\right|^2, \tag{6}$$

where

$$D_V=m_V^2-s-i\sqrt{s}\Gamma_V(s),$$

$$\Gamma_V(s)=\Gamma(V\to 3\pi,s)+\Gamma(V\to\eta\gamma,s)+\Gamma(V\to\pi^0\gamma,s)+\Gamma(V\to K^+K^-,s)+\Gamma(V\to K_SK_L,s)+\Gamma(V\to\pi^+\pi^-,s). \tag{7}$$

Here V denotes the vector mesons ρ,ω,ϕ; $q_{K^+K^-}(s)$, $q_{K_SK_L}(s)$ are kaon momenta, $W(s)$ is a phase space factor including $\rho\pi$ intermediate state [15], $A_{K^+K^-}$, $A_{K_SK_L}$, and $A_{3\pi}$ are amplitudes corresponding to contributions additional to the conventional VDM (for example ρ, ω, and ϕ primes), and $\chi_{\phi-\omega}$ and $\phi_{K\bar{K}}$ are the relative interference phases. The $\phi_{K\bar{K}}$ and $\chi_{\phi-\omega}$ phases are equal to 180° in the framework of the naive quark model.

The partial decay width dependences on energy are written as

$$\Gamma(V\to 3\pi,s)=\frac{|g_{V\rho\pi}|^2}{4\pi}W(s),$$

$$\Gamma(V\to PP,s)=\frac{|g_{VPP}|^2}{6\pi s}q^3_{PP}(s),$$

$$\Gamma(V\to P\gamma,s)=\frac{1}{3}|g_{VP\gamma}|^2q^3_{P\gamma}(s), \tag{8}$$

where P denotes the pseudoscalar meson π or K.

The coupling constants are determined through the decay branching ratios in the following way:

$$|g_{V\gamma}|=\left[\frac{3m_V^3\Gamma_VB(V\to e^+e^-)}{4\pi\alpha}\right]^{1/2},$$

$$|g_{VP\gamma}|=\left[\frac{3\Gamma_VB(V\to P\gamma)}{q^3_{P\gamma}(m_V)}\right]^{1/2},$$

$$|g_{V\rho\pi}|=\left[\frac{4\pi\Gamma_VB(V\to\rho\pi)}{W(m_V)}\right]^{1/2},$$

$$|g_{VPP}|=\left[\frac{6\pi m_V^2\Gamma_VB(V\to PP)}{q^3_{PP}(m_V)}\right]^{1/2},$$

$$|g_{\omega(\rho)K^+K^-}|=\frac{1}{\sqrt{2}}|g_{\phi K^+K^-}|,$$

$$|g_{\omega(\rho)K_SK_L}|=\frac{1}{\sqrt{2}}|g_{\phi K_SK_L}|. \tag{9}$$

Here $\Gamma_V=\Gamma_V(m_V)$. To restrict the growth of the partial width $\Gamma(\omega\to 3\pi,s)$ with energy, the form factor is usually included [15] in the $g_{\omega\rho\pi}$ coupling constant, $g_{\omega\rho\pi}\to g_{\omega\rho\pi}\sqrt{C_{\omega\rho\pi}(s)}$, where

$$C_{\omega\rho\pi}(s)=\left[\frac{1+(R_{\omega\rho\pi}m_\omega)^2}{1+(R_{\omega\rho\pi}\sqrt{s})^2}\right]^2. \tag{10}$$

We did not use this form factor for the experimental data approximation in this work: the parameter $R_{\omega\rho\pi}$ was set to zero.

The Coulomb interaction of the charged kaons in the final state was taken into account by multiplying the coupling constant $g_{\phi K^+K^-}$ by the appropriate form factor, $g_{\phi K^+K^-}\to g_{\phi K^+K^-}\sqrt{Z(s)/Z(m_\phi)}$, where [16]

$$Z(s)=1+\alpha\pi\frac{1+v^2}{2v},\quad v=\left(1-\frac{4m^2_{K^\pm}}{s}\right)^{1/2}.$$

In the vicinity of the ϕ-meson peak, the value $Z(s)$ is nearly constant and the influence of the $\sqrt{Z(s)/Z(m_\phi)}$ form factor on the resonance width and mass is negligible.

For the experimental data approximation, theoretical cross sections were reduced to the following expressions:

$$\sigma_{K^+K^-}(s)=\frac{1}{s^{5/2}}\frac{q^3_{K^+K^-}(s)}{q^3_{K^+K^-}(m_\phi)}\left|\frac{\Gamma_\phi m_\phi^3\sqrt{\sigma(\phi\to K^+K^-)m_\phi}}{D_\phi(s)}e^{i\phi_{K\bar{K}}}-\frac{\sqrt{\Gamma_\phi\Gamma_\omega m_\omega^3 m_\phi^2 6\pi B(\omega\to e^+e^-)B(\phi\to K^+K^-)}}{D_\omega(s)}\right.$$
$$\left.-\frac{\sqrt{\Gamma_\phi\Gamma_\rho m_\rho^3 m_\phi^2 6\pi B(\rho\to e^+e^-)B(\phi\to K^+K^-)}}{D_\rho(s)}+A^0_{K^+K^-}\right|^2, \tag{11}$$

$$\sigma_{K_SK_L}(s)=\frac{1}{s^{5/2}}\frac{q^3_{K_SK_L}(s)}{q^3_{K_SK_L}(m_\phi)}\left|\frac{\Gamma_\phi m_\phi^3\sqrt{\sigma(\phi\to K_SK_L)m_\phi}}{D_\phi(s)}e^{i\phi_{K\bar{K}}}-\frac{\sqrt{\Gamma_\phi\Gamma_\omega m_\omega^3 m_\phi^2 6\pi B(\omega\to e^+e^-)B(\phi\to K_SK_L)}}{D_\omega(s)}\right.$$
$$\left.+\frac{\sqrt{\Gamma_\phi\Gamma_\rho m_\rho^3 m_\phi^2 6\pi B(\rho\to e^+e^-)B(\phi\to K_SK_L)}}{D_\rho(s)}+A^0_{K_SK_L}\right|^2, \tag{12}$$

$$\sigma_{3\pi}(s)=\frac{1}{s^{3/2}}\frac{W(s)}{W(m_\phi)}\left|\frac{\Gamma_\phi m_\phi^2\sqrt{\sigma(\phi\to 3\pi)m_\phi}}{D_\phi(s)}e^{i\chi_{\phi\omega}}+\sqrt{\frac{W(m_\phi)}{W(m_\omega)}}\frac{\Gamma_\omega m_\omega^2\sqrt{\sigma(\omega\to 3\pi)m_\omega}}{D_\omega(s)}\sqrt{C_{\omega\rho\pi}(s)}+A^0_{3\pi}\right|^2, \tag{13}$$

where

$$\sigma(V\to X)=\frac{12\pi B(V\to e^+e^-)B(V\to X)}{m_V^2},$$

and $A^0_{K^+K^-}$, $A^0_{K_SK_L}$, $A^0_{3\pi}$ are complex constants, corresponding to the contributions of the higher radial excitations of the ρ, ω, and ϕ mesons in the cross section [17,18,21].

V. FITTING OF THE EXPERIMENTAL DATA

The experimental cross section $\sigma(s)$ can be calculated as follows:

$$\sigma(s)=\frac{N(s)}{IL(s)\epsilon(s)[1+\delta_{rad}(s)]}, \tag{14}$$

where $N(s)$ is the number of selected events, $IL(s)$ is the integrated luminosity, $\epsilon(s)$ is the detection efficiency, and $\delta_{rad}(s)$ is the radiative correction calculated according to Ref. [19]. The cross sections were fitted with the theoretical functions and the values of parameters and their errors were obtained using the procedure described in Ref. [20] which takes into account the beam energy spread and the error in the beam energy determination.

For the approximation of the $e^+e^-\to 3\pi$ cross section, to take into account the detection efficiency dependence $\epsilon(E_\gamma)$ on the emitted γ-quantum energy (Fig. 11), in the formula (14) the factor $\epsilon(s)[1+\delta_{rad}(s)]$ was replaced with the following expression:

$$\frac{\int_0^{E_\gamma^{max}}\sigma(s,E_\gamma)F(s,E_\gamma)\epsilon(E_\gamma)\mathrm{d}E_\gamma}{\sigma(s)}, \tag{15}$$

where E_γ is the emitted photon energy and $F(s,E_\gamma)$ is the electron ''radiator'' function [19].

A. Fitting of the $e^+e^-\to\pi^+\pi^-\pi^0$ cross section

The fitting of the $e^+e^-\to\pi^+\pi^-\pi^0$ cross section was performed with the m_ϕ, Γ_ϕ, $\sigma(\phi\to 3\pi)$, $A^0_{3\pi}$ and in some cases with the phase $\chi_{\phi-\omega}$ as free parameters. Approximations were performed under the following assumptions on the $\chi_{\phi-\omega}$ value:

(i) $\chi_{\phi-\omega}=180°$.

(ii) $\chi_{\phi-\omega}=180°+\Delta\chi_{\phi-\omega}(s)$.

(iii) $\chi_{\phi-\omega}$ is a free parameter.

Here the expression for $\Delta\chi_{\phi-\omega}(s)$ was taken from Ref. [24] and it is equal to $\Delta\chi_{\phi-\omega}(m_\phi)\simeq -17°$, when $s=m_\phi^2$.

The results of the fit are shown in Table VI. The first three variants correspond to the case when both the real and imaginary parts of the $A^0_{3\pi}$ amplitude were free parameters. The value of the $\mathrm{Re}(A^0_{3\pi})$ differs from zero by more than three standard deviations. The value of $\mathrm{Im}(A^0_{3\pi})$ is consistent with zero. Then the imaginary part was fixed at $\mathrm{Im}(A^0_{3\pi})=0$ and only the $\mathrm{Re}(A^0_{3\pi})$ was taken as a free parameter (four to six variants in Table VI). The values of m_ϕ and Γ_ϕ do not depend on the theoretical model. The model dependence of the parameter $\sigma(\phi\to 3\pi)$ is about $\sim 10\%$ and the difference of its values for variants 4 and 5 is much greater than the errors. The energy dependence of the $e^+e^-\to 3\pi$ cross section for variant 5 is shown in Fig. 12. At the right side from the resonance peak, the cross section has a minimum due to the interference of the ϕ-meson amplitude with the nonresonant part of the cross section. The cross section value does not actually depend on the model parameters in the energy range $\sqrt{s}=984$–1028 MeV, but in the region of the interference minimum at $\sqrt{s}=1040$ MeV, it can differ by a factor of 2 for different models (Fig. 13). This uncertainty is connected with the difference in the values of $\delta_{rad}(s)$ correction in Eq. (14), calculated for different models.

B. Fitting of the $e^+e^-\to K\bar{K}$ cross sections

The $e^+e^-\to K^+K^-$ and K_SK_L cross sections were fitted with m_ϕ, Γ_ϕ, $\sigma(\phi\to K^+K^-)$, $\sigma(\phi\to K_SK_L)$ as free param-

TABLE VI. Fit results for the process $e^+e^-\to\pi^+\pi^-\pi^0$. The column number N corresponds to the different variants of choice of the phase $\chi_{\phi-\omega}$ and the imaginary part of the amplitude $\mathrm{Im}(A^0_{3\pi})$. Here $\Psi_{\phi-\omega}(s)=180°+\Delta\chi_{\phi-\omega}(s)$ is the phase value predicted in Ref. [24].

N	1	2	3	4	5	6
$m_\phi-1000$ (MeV)	19.41 ± 0.03	19.42 ± 0.03	19.41 ± 0.03	19.41 ± 0.03	19.42 ± 0.03	19.42 ± 0.03
Γ_ϕ (MeV)	4.18 ± 0.06	4.18 ± 0.06	4.18 ± 0.06	4.18 ± 0.06	4.19 ± 0.06	4.18 ± 0.06
$\sigma(\phi\to3\pi)$ (nb)	$668\pm^{47}_{16}$	$657\pm^{33}_{16}$	668 ± 24	704 ± 8	661 ± 7	$666\pm^{52}_{18}$
$\mathrm{Re}(A^0_{3\pi})\times10^3$ ($\mathrm{MeV}^{1/2}$)	$-54\pm^{10}_{5}$	$-48\pm^{15}_{6}$	-53 ± 6	-47 ± 3	-47 ± 3	-47 ± 3
$\mathrm{Im}(A^0_{3\pi})\times10^3$ ($\mathrm{MeV}^{1/2}$)	$-35\pm^{40}_{14}$	$-4\pm^{30}_{10}$	-33 ± 60	0	0	0
$\chi_{\phi-\omega}$ (deg)	180	$\Psi_{\phi-\omega}(s)$	178 ± 27	180	$\Psi_{\phi-\omega}(s)$	$165\pm^{20}_{6}$
χ^2/N_{df}	20.39/27	20.46/27	20.39/26	20.56/28	20.49/28	20.49/27

eters. The parameters $A^0_{K^+K^-}$, $A^0_{K_SK_L}$, and $\phi_{K\bar{K}}$ were either fixed [$\phi_{K\bar{K}}=180°$ and $A^0_{K^+K^-}(A^0_{K_SK_L})=0$] or were free parameters. In particular, various fits were performed under the following assumptions:

(1) $\phi_{K\bar{K}}=180°$, $A^0_{K^+K^-}=A^0_{K_SK_L}=0$.

(2) $\phi_{K\bar{K}}$ was free parameter, $A^0_{K^+K^-}=A^0_{K_SK_L}=0$.

(3) $\phi_{K\bar{K}}$ and $\mathrm{Re}(A^0_{K^+K^-})$, $\mathrm{Re}(A^0_{K_SK_L})$ were free parameters.

(4) $\phi_{K\bar{K}}=180°$, $\mathrm{Re}(A^0_{K^+K^-})$, $\mathrm{Re}(A^0_{K_SK_L})$, $\mathrm{Im}(A^0_{K^+K^-})$, $\mathrm{Im}(A^0_{K_SK_L})$ were free parameters.

(5) $\phi_{K\bar{K}}=180°$, $\mathrm{Re}(A^0_{K^+K^-})$, and $\mathrm{Re}(A^0_{K_SK_L})$ were free parameters.

The results of the fit are shown in Tables VII and VIII.

For the $e^+e^-\to K^+K^-$ process, the phase $\phi_{K\bar{K}}$ agrees with the theoretically predicted value 180°. The imaginary part of the $A^0_{K^+K^-}$ amplitude is consistent with zero, and its real part is different from zero by about only one standard deviation (variants 4 and 5 in Table VII). The values of m_ϕ and Γ_ϕ do not depend on the applied theoretical model. The value of $\sigma(\phi\to K^+K^-)$ varies by 2% for different variants, but these biases are less than its error. The cross section is

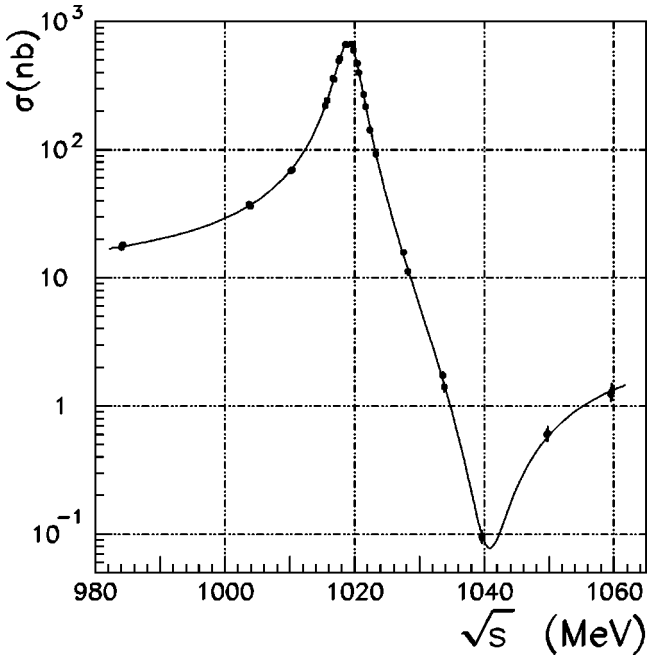

FIG. 12. The $e^+e^-\to\pi^+\pi^-\pi^0$ cross section. The dots are experimental data; the curve is the fit.

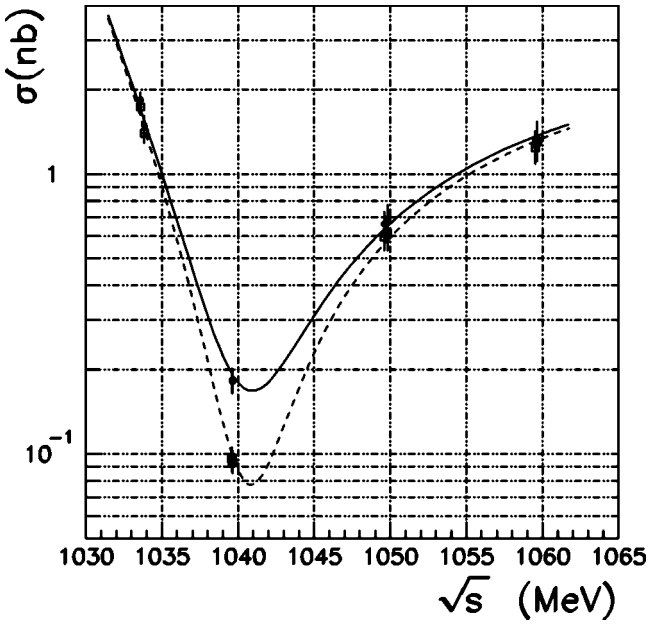

FIG. 13. The $e^+e^-\to\pi^+\pi^-\pi^0$ cross section in the interference minimum region. Solid curve and dots: fit with $\chi_{\phi-\omega}=180°$, $\mathrm{Im}(A^0_{3\pi})=0$. Dashed curve and squares: the fit with $\chi_{\phi-\omega}=180°+\Delta\chi_{\phi-\omega}(s)$, $\mathrm{Im}(A^0_{3\pi})=0$.

TABLE VII. Fit results for the process $e^+e^-\to K^+K^-$. The column number N corresponds to the different variants of choice of the phase $\phi_{K\bar{K}}$ and the real and imaginary parts of the amplitude $\mathrm{Re}(A^0_{K^+K^-})$, $\mathrm{Im}(A^0_{K^+K^-})$.

N	1	2	3	4	5
m_ϕ (MeV)	1019.46 ± 0.03	1019.46 ± 0.03	1019.44 ± 0.03	1019.44 ± 0.03	1019.44 ± 0.04
Γ_ϕ (MeV)	4.28 ± 0.06	4.26 ± 0.06	4.22 ± 0.08	4.22 ± 0.08	4.22 ± 0.08
$\sigma(\phi\to K^+K^-)$ (nb)	1940 ± 31	1962 ± 38	$1972\pm^{63}_{58}$	1969 ± 64	1950 ± 32
$\phi_{K\bar{K}}$ (deg)	180	157 ± 24	$156\pm^{51}_{39}$	180	180
$\mathrm{Re}(A^0_{K^+K^-})$ ($\mathrm{MeV}^{3/2}$)	0	0	$4.7\pm^{14}_{5.3}$	$7.1\pm^{25}_{7}$	5.9 ± 4.8
$\mathrm{Im}(A^0_{K^+K^-})$ ($\mathrm{MeV}^{3/2}$)	0	0	0	12 ± 33	0
χ^2/N_{df}	22.15/25	21.2/24	20.45/23	20.54/23	20.65/24

almost independent of the applied model (Fig. 14).

The data for the $e^+e^-\to K_SK_L$ reaction obtained in charged and neutral modes were fitted simultaneously. For this process the phase $\phi_{K\bar{K}}$ is different from the expected 180° by more then five standard deviations and is close to 90° (variant 2 in Table VIII). The imaginary part of the $A^0_{K_SK_L}$ amplitude is consistent with zero, and its real part is different from zero by about two standard deviations (variants 5 and 4 in Table VIII). The parameters m_ϕ and Γ_ϕ are slightly dependent on the theoretical assumptions. The value of $\sigma(\phi\to K_SK_L)$ varies by 2% for different variants and is shown in Fig. 15. The cross section is almost insensitive to the choice of the model.

C. Combined fitting of the cross sections

To obtain the ϕ-meson production cross section and branching ratios of the main decay modes, the combined fitting of the experimental data, taking into account the $e^+e^-\to\eta\gamma$ cross section also, was carried out. As this work does not contain the analysis of the $e^+e^-\to\eta\gamma$ reaction, it was natural to use the cross section $\sigma(\phi\to\eta\gamma)$ from the previous SND measurements presented in Ref. [25]. In Ref. [25] the correction $\delta_{over}=0.97\pm0.03$ to the detection efficiency was not applied. The value $\sigma(\phi\to\eta\gamma)=53.2\pm2$ nb, presented there, was increased by 3% and the value 54.8 ± 2.1 nb was used in the fit. The results of the fit, for the different model assumptions, are shown in Table IX. In all fits $\mathrm{Im}(A^0_{K^+K^-})=0$, $\mathrm{Im}(A^0_{K_SK_L})=0$, and $\mathrm{Im}(A^0_{3\pi})=0$ were set.

Using these data, the following ϕ-meson parameters were obtained: the ϕ-meson production cross section

$$\sigma(\phi)=\sum_X \sigma(\phi\to X),$$

TABLE VIII. Fit results for the process $e^+e^-\to K_SK_L$. The column number N corresponds to the different variants of choice of the phase $\phi_{K\bar{K}}$ and the real and imaginary parts of the amplitude $\mathrm{Re}(A^0_{K_SK_L})$, $\mathrm{Im}(A^0_{K_SK_L})$ choice.

N	1	2	3	4	5
m_ϕ (MeV)	1019.40 ± 0.02	1019.38 ± 0.02	1019.38 ± 0.02	1019.38 ± 0.02	1019.38 ± 0.02
Γ_ϕ (MeV)	4.20 ± 0.04	4.15 ± 0.04	4.15 ± 0.05	4.16 ± 0.04	4.16 ± 0.04
$\sigma(\phi\to K_SK_L)$ (nb)	1454 ± 12	1436 ± 12	$1450\pm^{73}_{51}$	$1440\pm^{76}_{40}$	1458 ± 12
$\phi_{K\bar{K}}$ (deg)	180	102 ± 14	120 ± 51	180	180
$\mathrm{Re}(A^0_{K_SK_L})$ ($\mathrm{MeV}^{3/2}$)	0	0	$8\pm^{30}_{40}$	$4\pm^{5}_{7}$	5.7 ± 2.8
$\mathrm{Im}(A^0_{K_SK_L})$ ($\mathrm{MeV}^{3/2}$)	0	0	0	$-3\pm^{50}_{26}$	0
χ^2/N_{df}	64.11/57	59.95/56	59.94/55	59.95/55	59.96/56

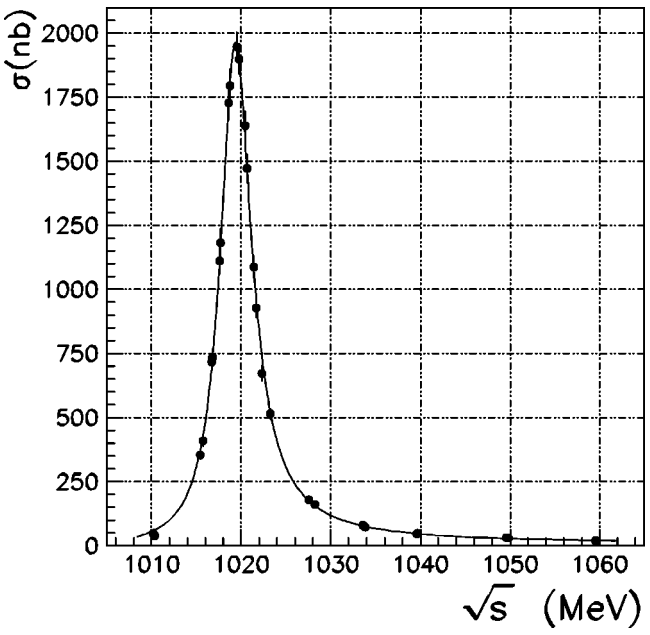

FIG. 14. The $e^+e^-\to K^+K^-$ cross section. The dots are experimental data; the curve is the fit.

$$X=K^+K^-,K_SK_L,\pi^+\pi^-\pi^0,\eta\gamma, \tag{16}$$

the branching ratios of the main decay modes

$$B(\phi\to X)=\frac{\sigma(\phi\to X)}{\sigma(\phi)}, \tag{17}$$

and the branching ratio of the decay into an e^+e^- pair:

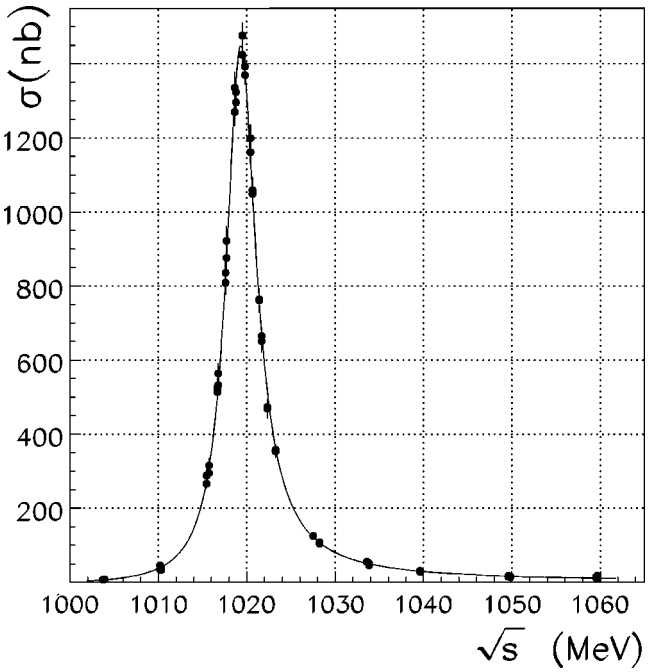

FIG. 15. The $e^+e^-\to K_SK_L$ cross section. The dots are experimental data; the curve is the fit.

$$B(\phi\to e^+e^-)=\frac{\sigma(\phi)m_\phi^2}{12\pi}. \tag{18}$$

The final results are

$$B(\phi\to e^+e^-)=(2.93\pm0.02\pm0.14\pm0.02)\times10^{-4},$$

$$B(\phi\to K^+K^-)=47.6\pm0.3\pm1.6\pm0.3\,\%,$$

$$B(\phi\to K_SK_L)=35.1\pm0.2\pm1.2\pm0.3\,\%,$$

$$B(\phi\to3\pi)=15.9\pm0.2\pm0.7\pm0.4\,\%,$$

$$B(\phi\to\eta\gamma)=1.33\pm0.03\pm0.05\pm0.01\,\%.$$

These values correspond to the the fit where $\chi_{\phi-\omega}=180°+\Delta\chi_{\phi-\omega}(s)$, $\phi_{K\bar{K}}=180°$, $\mathrm{Im}(A^0_{3\pi})=0$, $A^0_{K_SK_L}=0$, and $A^0_{K^+K^-}=0$ (variant 2 in Table IX). The third error is a model uncertainty. The presented values are in good agreement with the world average and with other experimental data (Table X). Using the SND data, the following coupling constants were calculated: $|g_{\phi\gamma}|=6538\pm156$ MeV^2, $|g_{\phi K^+K^-}|=4.391\pm0.078$, $|g_{\phi K_SK_L}|=4.664\pm0.086$, $|g_{\phi\rho\pi}|=0.815\pm0.021$ GeV^{-1}, and $|g_{\phi\eta\gamma}|=0.0593\pm0.0013$ GeV^{-1}.

The measured cross sections are given in Table XI. The systematic errors of the $e^+e^-\to K^+K^-$, $e^+e^-\to\pi^+\pi^-\pi^0$ cross sections and of the related parameters $\sigma(\phi\to K^+K^-)$, $\sigma(\phi\to3\pi)$ are 7.1% and 5%, respectively, and include the systematic uncertainties in the detection efficiency and luminosity determinations. For the $e^+e^-\to K_SK_L$ cross section, the systematic error is 4.2% in the charged mode and 4.0% in the neutral mode. The systematic error of the parameter $\sigma(\phi\to K_SK_L)$ is 3.2%.

VI. DISCUSSION

The ϕ-meson mass and width measured in the three studied main decay modes are consistent with each other. The measurements of the ϕ-meson parameters in all channels have high accuracy. Let us mention that all these processes have different energy dependence for detection efficiency. The dependence of the mass value on the applied theoretical model is less than the measurement accuracy. As a result of the combined approximation, we find

$$m_\phi=1019.42\pm0.02\pm0.04\ \text{MeV},$$

where the systematic error of 0.04 MeV is attributed to the possible common shift of the collider energy scale. This value is consistent with the world average: 1019.417 ± 0.014 MeV [21]. The value of the total ϕ-meson width, obtained by using different models, can vary from 4.18 to 4.21 MeV and was found to be

$$\Gamma_\phi=4.21\pm0.03\pm0.02\ \text{MeV}$$

(the systematic error 0.02 MeV is due to model dependence), and differs from the world average 4.458 ± 0.032 MeV [21]

TABLE IX. Results of the combined fit for the processes $e^+e^-\to K\bar{K}$ and 3π. The column number N corresponds to the different variants of choice of the phases $\phi_{K\bar{K}}$, $\chi_{\phi-\omega}$ and the real parts of the amplitudes $\mathrm{Re}(A^0_{K^+K^-})$, $\mathrm{Re}(A^0_{K_SK_L})$, $\mathrm{Re}(A^0_{3\pi})$.

N	1	2	3	4	5
$m_\phi-1000$ (MeV)	19.417 ± 0.014	19.419 ± 0.014	19.419 ± 0.014	19.418 ± 0.014	19.40 ± 0.02
Γ_ϕ (MeV)	4.21 ± 0.04	4.21 ± 0.03	4.21 ± 0.03	4.21 ± 0.03	4.18 ± 0.03
$\sigma(\phi\to K_SK_L)$ (nb)	1451 ± 10	1451 ± 10	1451 ± 10	1441 ± 12	1455 ± 10
$\sigma(\phi\to K^+K^-)$ (nb)	1968 ± 20	1968 ± 20	1967 ± 20	1994 ± 27	1961 ± 21
$\sigma(\phi\to 3\pi)$ (nb)	701 ± 6	659 ± 6	$664\pm^{48}_{18}$	702 ± 6	705 ± 6
$\mathrm{Re}(A^0_{K^+K^-})$ ($\mathrm{MeV}^{3/2}$)	0	0	0	0	8.6 ± 3.9
$\mathrm{Re}(A^0_{K_SK_L})$ ($\mathrm{MeV}^{3/2}$)	0	0	0	0	4.3 ± 2.5
$\mathrm{Re}(A^0_{3\pi})\times10^3$ ($\mathrm{MeV}^{1/2}$)	-46 ± 3	-46 ± 3	-46 ± 3	-46 ± 3	-46 ± 3
$\chi_{\phi-\omega}$ (deg)	180	$180+\Delta\chi_{\phi-\omega}(s)$	$165\pm^{19}_{7}$	180	180
$\phi_{K\bar{K}}$ (deg)	180	180	180	$147\pm^{27}_{16}$	180
χ^2/N_{df}	110.29/114	110.09/114	110.1/113	108.67/113	103.39/111

by 4.8 standard deviations and from the most precise measurement $\Gamma_\phi=4.477\pm0.036\pm0.022$ MeV [8] by 4.5 standard deviations.

The $e^+e^-\to\pi^+\pi^-\pi^0$ process, as the approximation showed, cannot be described by only ϕ- and ω-meson decays and it is necessary to include additional amplitude $A^0_{3\pi}$, which can be explained as a contribution of the higher resonances. The presence of such an amplitude is also expected from the experimental data on the $e^+e^-\to\pi^+\pi^-\pi^0$ cross section measured by the SND detector [26] in the energy region above the ϕ resonance, which cannot be described with the conventional VDM. The value of the amplitude $A^0_{3\pi}=0.046\pm0.003$ $\mathrm{MeV}^{1/2}$ (Table IX) is only 2 times lower than the real part of ω-meson amplitude in the vicinity of the ϕ-meson peak, $\mathrm{Re}(A_\omega)\simeq0.09$ $\mathrm{MeV}^{1/2}$, and approximately equals its imaginary part $\mathrm{Im}(A_\omega)\simeq0.05$ $\mathrm{MeV}^{1/2}$. The presence of the $A^0_{3\pi}$ amplitude prevents a test of the deviation of the $\chi_{\omega-\phi}$ phase from 180°. Both $\chi_{\phi-\omega}=180°$ and $180°+\Delta\chi_{\phi-\omega}(s)$ [24] are consistent with the experimental data. If the $\chi_{\phi-\omega}$ phase is considered to be a free parameter with no energy dependence, then its fitted value is $178°\pm27°$ for free real and imaginary parts of $A^0_{3\pi}$ (variant 5 in Table VI) and $165°\pm^{19°}_{7}$ if $\mathrm{Im}(A^0_{3\pi})=0$ is set (variant 3 in Table IX).

TABLE X. The comparison of the main results of this work with PDG data [21] and results of the other experiments [5,8].

	SND	Other data
$\sigma(\phi\to K_SK_L)$ (nb)	1451 ± 49	1367 ± 26 [8]
$\sigma(\phi\to K^+K^-)$ (nb)	1968 ± 142	2001 ± 105 [5]
$\sigma(\phi\to3\pi)$ (nb)	659 ± 35	654 ± 40 [5]
$B(\phi\to e^+e^-)\times10^4$	2.93 ± 0.14	2.91 ± 0.07 [21]
$B(\phi\to K^+K^-)$ (%)	47.6 ± 1.7	49.2 ± 0.7 [21]
$B(\phi\to K_SK_L)$ (%)	35.1 ± 1.3	33.8 ± 0.6 [21]
$B(\phi\to3\pi)$ (%)	15.9 ± 0.8	15.5 ± 0.6 [21]
$B(\phi\to\eta\gamma)$ (%)	1.33 ± 0.06	1.297 ± 0.033 [21]
m_ϕ MeV	1019.42 ± 0.05	1019.417 ± 0.014 [21]
Γ_ϕ MeV	4.21 ± 0.04	4.458 ± 0.032 [21]

The parameter

$$\sigma(\phi\to3\pi)=659\pm6\pm33\pm^{20}_{5}\ \text{nb}$$

has a rather large model error ($\pm^{20}_{5}$ nb), due to the uncertainty in the choice of the phase $\chi_{\omega-\phi}$. The quoted value of the $\sigma(\phi\to3\pi)$ corresponds to the choice $\chi_{\omega-\phi}=180°+\Delta\chi_{\phi-\omega}(s)$ and $\mathrm{Im}(A^0_{3\pi})=0$. It agrees with other measurements, for example, $\sigma(\phi\to3\pi)=619\pm39\pm12$ from Ref. [6] and $\sigma(\phi\to3\pi)=654\pm26\pm30$ from Ref. [5].

In case of the $e^+e^-\to K^+K^-$ and K_SK_L processes, the $\mathrm{Im}(A^0_{K^+K^-})$, $\mathrm{Im}(A^0_{K_SK_L})$ agree with zero (variant 4 in Tables VII and VIII) and $\mathrm{Re}(A^0_{K^+K^-})$, $\mathrm{Re}(A^0_{K_SK_L})$ deviates from zero by about two standard deviations (variant 5, Table IX). The phase $\phi_{K\bar{K}}$ extracted from the combined fit or from the fitting of the $e^+e^-\to K^+K^-$ process is consistent with 180°

TABLE XI. The $e^+e^-\to K\overline{K}$ and 3π cross sections. First error is statistical and the second is model uncertainty. The systematic errors are 7.1% for $e^+e^-\to K^+K^-$, 4% and 4.2% for $e^+e^-\to K_SK_L$ at charged and neutral modes, and 5% for $e^+e^-\to 3\pi$.

$\sqrt{s}$	$\sigma_{K^+K^-}$	$\sigma_{K_SK_L}$ (charged mode)	$\sigma_{K_SK_L}$ (neutral mode)	$\sigma_{3\pi}$
		SCAN PHI9801		
984.21				18.1 ± 0.9
1003.91		7.7 ± 3.0	7.7 ± 1.0	36.2 ± 1.3
1010.17	48.1 ± 13.3	45.2 ± 6.1	34.0 ± 2.8	68.5 ± 2.4
1015.75	409.0 ± 20.3	315.5 ± 20.2	294.5 ± 13.3	243.1 ± 7.5
1016.68	717.1 ± 32.3	525.5 ± 25.7	513.1 ± 20.6	358.9 ± 10.6
1017.59	1112.0 ± 51.8	836.3 ± 37.6	809.1 ± 32.5	493.6 ± 14.9
1018.78	1794.1 ± 64.8	1324.7 ± 40.4	1295.0 ± 33.7	658.6 ± 11.6
1019.79	1898.1 ± 56.9	1388.4 ± 36.2	1372.4 ± 23.9	595.5 ± 14.1
1020.65	1471.9 ± 54.5	1053.0 ± 35.6	1051.9 ± 30.3	399.8 ± 14.5
1021.68	928.4 ± 37.7	648.0 ± 29.0	667.2 ± 22.3	217.4 ± 8.5
1023.27	514.4 ± 20.0	352.0 ± 16.7	359.5 ± 11.7	92.2 ± 3.4
1028.23	161.1 ± 6.0	103.0 ± 7.0	108.1 ± 4.0	$11.2\pm0.65\pm0.036$
1033.84	72.9 ± 2.9	45.1 ± 4.0	52.0 ± 2.1	$1.400\pm0.113\pm^{0.100}_{0.060}$
1039.59	47.4 ± 2.0	$28.3\pm3.1\pm0.1$	$31.0\pm1.5\pm0.4$	$0.096\pm0.010\pm^{0.09}_{0.05}$
1049.81	29.0 ± 1.5	$13.3\pm2.1\pm0.6$	$16.4\pm0.9\pm0.5$	$0.613\pm0.081\pm^{0.080}_{0.040}$
1059.66	18.6 ± 1.2	$17.0\pm2.6\pm2.2$	$11.0\pm0.7\pm0.5$	$1.304\pm0.194\pm^{0.070}_{0.040}$
		SCAN PHI9802		
984.02				17.3 ± 0.8
1003.71		7.4 ± 2.9	6.7 ± 1.0	37.6 ± 1.4
1010.34	38.7 ± 12.8	40.0 ± 6.3	33.7 ± 2.7	69.5 ± 2.5
1015.43	354.2 ± 17.2	288.3 ± 17.2	265.9 ± 11.2	220.0 ± 6.5
1016.78	734.7 ± 34.2	564.0 ± 27.1	532.6 ± 21.7	353.6 ± 11.1
1017.72	1181.8 ± 54.7	923.1 ± 39.5	875.1 ± 34.1	515.0 ± 15.3
1018.62	1726.7 ± 65.8	1337.1 ± 42.7	1268.5 ± 36.3	664.2 ± 13.1
1019.51	1946.2 ± 56.7	1473.8 ± 34.7	1426.3 ± 21.6	667.0 ± 11.8
1020.43	1639.6 ± 56.8	1193.1 ± 37.2	1165.2 ± 30.6	471.2 ± 15.5
1021.41	1087.2 ± 42.2	757.5 ± 32.5	767.0 ± 24.7	270.1 ± 9.9
1022.32	672.9 ± 29.8	465.9 ± 24.5	475.4 ± 17.7	142.9 ± 6.1
1027.52	179.6 ± 6.9	123.8 ± 7.8	125.3 ± 4.2	$15.803\pm0.752\pm0.037$
1033.58	79.9 ± 2.9	55.4 ± 4.2	54.8 ± 2.0	$1.737\pm0.113\pm^{0.100}_{0.07}$
1039.64	48.7 ± 1.9	$27.3\pm3.0\pm0.1$	$29.6\pm1.4\pm0.4$	$0.094\pm0.009\pm^{0.08}_{0.06}$
1049.60	31.2 ± 1.5	$15.0\pm2.1\pm0.7$	$17.5\pm0.9\pm0.5$	$0.595\pm0.062\pm^{0.080}_{0.04}$
1059.52	20.9 ± 1.2	$14.0\pm2.5\pm1.8$	$11.7\pm0.7\pm0.5$	$1.238\pm0.151\pm^{0.060}_{0.04}$

(variants 2 and 4 in Tables VII and IX), but the fitting of the $e^+e^-\to K_SK_L$ data gives the phase value close to 90°. Such a result can be attributed to the uncertainty of the nonresonant contributions to the cross section and was used to estimate the model error in the cross section determination. The results

$$\sigma(\phi\to K^+K^-)=1968\pm20\pm140 \text{ nb},$$

$$\sigma(\phi\to K_SK_L)=1451\pm10\pm48 \text{ nb}$$

agree with the world average [21].

Isotopic symmetry predicts the equality of the $g_{\phi K^+K^-}$ and $g_{\phi K_SK_L}$ coupling constants. The electromagnetic interactions of charged kaons in the final state lead to the relation $g_{\phi K^+K^-}/\sqrt{Z(m_\phi)}=g_{\phi K_SK_L}$. Using the Particle Data Group (PDG) data, [21] one can find

$$\frac{g_{\phi K^+K^-}}{g_{\phi K_SK_L}}\frac{1}{\sqrt{Z(m_\phi)}}=\sqrt{\left(\frac{B(\phi\to K^+K^-)q^3_{K_SK_L}(m_\phi)}{B(\phi\to K_SK_L)q^3_{K^+K^-}(m_\phi)}\right)\frac{1}{Z(m_\phi)}}$$
$$=0.95\pm0.01. \quad (19)$$

This value differs considerably (five standard deviations) from the expected value of unity. It is possible that the Coulomb correction is less than expected due to finite dimensions of the final particles. A similar problem in the Υ_{4s}

$\rightarrow B\bar{B}$ decay was discussed in Refs. [22,23]. Quite recently the ratio of the constants $g_{\phi K^+K^-}$ and $g_{\phi K_S K_L}$ was discussed in Ref. [27], where it was suggested to study this ratio in e^+e^- annihilation around the ϕ-resonance peak. The drawback of this proposal is a very low sensitivity of such studies to the nonresonant contribution to the total cross section. The extracted coupling constant values depend on the nonresonant contribution to the total cross section from the ρ and ω mesons and from higher radial excitations (ρ', ω', ϕ', . . .). So one of the possible approaches to the solution of this problem can be a precise study of these contributions to the total cross section by means of the measurement of the $e^+e^- \rightarrow K\bar{K}$ cross section in a wide energy range. Unfortunately the SND data have rather high systematic errors, which preclude such studies, and they are accumulated in a rather narrow energy region. From SND data (Table IX) one can obtain

$$\frac{g_{\phi K^+K^-}}{g_{\phi K_S K_L}} \frac{1}{\sqrt{Z(m_\phi)}} = 0.92 \pm 0.03. \qquad (20)$$

This value agrees with the quoted world average, but is also consistent with the expected value of 1 (the difference is about 2.5 standard deviations).

VII. CONCLUSION

The main parameters of the ϕ resonance were obtained in experiments with the SND detector at the VEPP-2M collider. The integrated luminosity used was about 8.5 pb^{-1}. The processes $e^+e^- \rightarrow K^+K^-$, $e^+e^- \rightarrow K_S K_L$, and $e^+e^- \rightarrow \pi^+\pi^-\pi^0$ were studied. The measured cross sections were approximated within the VDM, taking into account ρ, ω, and ϕ mesons. Possible contributions from higher resonances ρ', ω', ϕ' were included as constant amplitudes. The ϕ-meson parameters obtained by the approximation (Table X) mainly agree with PDG data and have accuracies comparable with the world averages. The ϕ-meson total width was found to be 4.21 ± 0.04 MeV in contradiction to the PDG value 4.458 ± 0.032 MeV. For a good approximation of the $e^+e^- \rightarrow \pi^+\pi^-\pi^0$ cross section the additional contribution is strongly required, and its value is about 2 times lower than the real part of the ω-meson contribution. This contribution can be attributed to the higher resonances, for example, to the resonance structure found by SND [26].

ACKNOWLEDGMENTS

The authors are grateful to N.N. Achasov, E.P. Solodov, and S.I. Eidelman for useful discussions.

[1] G. Parrour *et al.*, Phys. Lett. B **364**, 362 (1976).
[2] A.D. Bukin *et al.*, Yad. Fiz. **27**, 976 (1978) [Sov. J. Nucl. Phys. **27**, 516 (1978)].
[3] A. Cordier *et al.*, Phys. Lett. B **364**, 13 (1980).
[4] S.I. Dolinsky *et al.*, Phys. Rep. **202**, 99 (1991).
[5] R.R. Akhmetshin *et al.*, Phys. Lett. B **364**, 199 (1995).
[6] B.R. Akhmetshin *et al.*, Phys. Lett. B **434**, 426 (1998).
[7] L.M. Kurdadze *et al.*, Report No. INP 84-07, Novosibirsk, 1984.
[8] R.R. Akhmetshin *et al.*, Phys. Lett. B **466**, 385 (1999).
[9] P. M. Ivanov *et al.*, Phys. Lett. **107B**, 297 (1981).
[10] V. E. Balakin *et al.*, Phys. Lett. **34B**, 328 (1971).
[11] A.N. Skrinsky, in Proceedings of the Workshop on Physics and Detectors for DAΦNE, Frascati, Italy, 1995, p. 3.
[12] M.N. Achasov *et al.*, Nucl. Instrum. Methods Phys. Res. A **449**, 125 (2000).
[13] R.R. Akhmetshin *et al.*, Report No. Budker INP 99-11, Novosibirsk, 1999.
[14] M.N. Achasov *et al.*, Phys. Lett. B **499**, 122 (1999).
[15] N.N. Achasov *et al.*, Yad. Fiz. **54**, 1097 (1991) [Sov. J. Nucl. Phys. **54**, 664 (1991)]; N.N. Achasov *et al.*, Int. J. Mod. Phys. A **7**, 3187 (1992).
[16] E. Cremmer and M. Gourdin, Nucl. Phys. **B9**, 451 (1969).
[17] N.N. Achasov and A.A. Kozhevnikov, Phys. Rev. D **55**, 2663 (1997); Yad. Fiz. **60**, 1131 (1997) [Phys. At. Nucl. **60**, 1011 (1997)].
[18] N.N. Achasov and A.A. Kozhevnikov, Phys. Rev. D **57**, 4334 (1998); Yad. Fiz. **60**, 2212 (1997) [Phys. At. Nucl. **60**, 2029 (1997)].
[19] E.A. Kuraev and V.S. Fadin, Yad. Fiz. **41**, 733 (1985) [Sov. J. Nucl. Phys. **41**, 466 (1985)].
[20] A.V. Bozhenok *et al.*, Report No. Budker INP 99-103, 1999.
[21] Particle Data Group, D.E. Groom *et al.*, Eur. Phys. J. C **15**, 1 (2000).
[22] D. Atwood and W.J. Marciano, Phys. Rev. D **41**, 1736 (1990).
[23] G.P. Lepage, Phys. Rev. D **42**, 3251 (1990).
[24] N.N. Achasov and A.A. Kozhevnikov, Phys. Rev. D **61**, 054005 (2000).
[25] M.N. Achasov *et al.*, Zh. Éksp. Teor. Fiz. **117**, 22 (2000) [JETP **90**, 17 (2000)].
[26] M.N. Achasov *et al.*, Phys. Lett. B **462**, 365 (1999).
[27] A. Bramon *et al.*, Phys. Lett. B **486**, 406 (2000).